


# Dielectrophoretic choking phenomenon in a converging-diverging microchannel for Janus particles

Teng Zhou<sup>1,\*</sup>, Xiang Ji<sup>1</sup>, Liuyong Shi<sup>1</sup>, Xianman Zhang<sup>1</sup>, Yongbo Deng<sup>2</sup>, Sang Woo Joo<sup>3,\*</sup>

<sup>1</sup>*Mechanical and Electrical Engineering College, Hainan University, Haikou 570228, Hainan, P. R. China*

<sup>2</sup>*Changchun Institute of Optics, Fine Mechanics and Physics (CIOMP), Chinese Academy of Science, Changchun 130033, Jilin, P. R. China*

<sup>3</sup>*School of Mechanical Engineering, Yeungnam University, Gyongsan 712-719, Korea*

\* Corresponding authors Email: [zhouteng@hainu.edu.cn](mailto:zhouteng@hainu.edu.cn)   
<http://orcid.org/0000-0002-8744-9083>✓

and [swjoo@yu.ac.kr](mailto:swjoo@yu.ac.kr)  <http://orcid.org/0000-0001-9102-4224>✓

## Abstract

The dielectrophoretic (DEP) choking phenomenon is revisited for Janus particles that are transported electrokinetically through a microchannel constriction by a direct-current (DC) electric field. The negative DEP force that would block a particle with a diameter significantly

Received: 08 31, 2018; Revised: 10 22, 2018; Accepted: 10 24, 2018

This article has been accepted for publication and undergone full peer review but has not been through the copyediting, typesetting, pagination and proofreading process, which may lead to differences between this version and the [Version of Record](#). Please cite this article as [doi: 10.1002/elps.201800368](https://doi.org/10.1002/elps.201800368).

This article is protected by copyright. All rights reserved.

smaller than that of the constriction at its inlet is seen to be relaxed by the rotation of the Janus particle in a direction that minimizes the magnitude of the DEP force. This allows the particle to pass through the constriction completely. An arbitrary Lagrangian-Eulerian (ALE) numerical method is used to solve the nonlinearly coupled electric field, flow field, and moving particle, and the DEP force is calculated by the Maxwell stress tensor (MST) method. The results show how Janus particles with non-uniform surface potentials overcome the DEP force and present new conditions for the DEP choking by a parametric study. Particle transportation through microchannel constrictions is ubiquitous, and particle surface properties are more likely to be non-uniform than not in practical applications. This study provides new insights of importance for non-uniform particles transported electrokinetically in a microdevice.

**Color online:** See article online to view Figs. 1–9 in color.

## Keywords

choking, dielectrophoresis (DEP), Janus particle, microchannel constriction

**Abbreviations:** arbitrary Lagrangian-Eulerian (ALE), electric double layer (EDL), Maxwell stress tensor (MST)

## 1. Introduction

The DC dielectrophoretic (DEP) phenomenon in microchannels has been studied intensively for decades, especially with the purpose of manipulating and separating micro-particles in motion [1-6]. The non-uniform geometry in a microchannel can distort the electric field distribution, and in turn, the distorted electric field can apply a DEP force on the particle. Therefore, the channels are designed to have various corresponding geometric

structures [7-11]. A converging-diverging structure is known to achieve convenient particle separation upon adjusting the applied electric field strength and the channel throat width, but particles with certain electric properties are blocked in the converging section, even though they seem sufficiently small for the constriction. This phenomenon is called DEP choking and has been studied recently. The conditions for the particle blockage have been revealed in terms of geometric, electric, and fluid-dynamic parameters [12-15].

Particles experiencing a negative DEP force that is large enough for their size to be blocked at the entrance of the constriction can still pass through it by deforming into shapes that are favorable for reducing the DEP force [12]. For particles with non-uniform surface properties, there is another way of overcoming the DEP force by rotating in such a way that the DEP force is minimized by facing the constriction “properly.” In the present study, this scenario is examined by studying the motion of Janus particles, which have different chemical or physical properties on the two hemispheres [16-18]. Based on the DEP particle manipulation principle, the non-uniform electric field polarizes the surface charge of the particles, and the magnitude of the field is related to the surface electric properties of Janus particles. Due to the different properties on the two hemispheres, the non-uniform electric field around the Janus particles does not have the same magnitude and produces various DEP forces on the particle surface, which can promote the DEP motion and self-rotation of the Janus particles.

This study investigates the DEP motion of Janus particles suspended in a non-uniform DC electric field, which is generated by the geometry of a converging-diverging micro-channel. Janus particles with different zeta potentials on the two hemispheres are employed. Based on the thin electric double layer (EDL) assumption, the arbitrary Lagrangian-Eulerian (ALE) numerical method [19-23] is used to solve the electric field, flow field, and suspended Janus particles simultaneously. The DEP force is accurately calculated by integrating the Maxwell stress tensor (MST), and fully coupled hydrodynamic force is considered. A parametric study was performed to determine new conditions for DEP choking for non-uniform particles in motion.

## 2. Theory

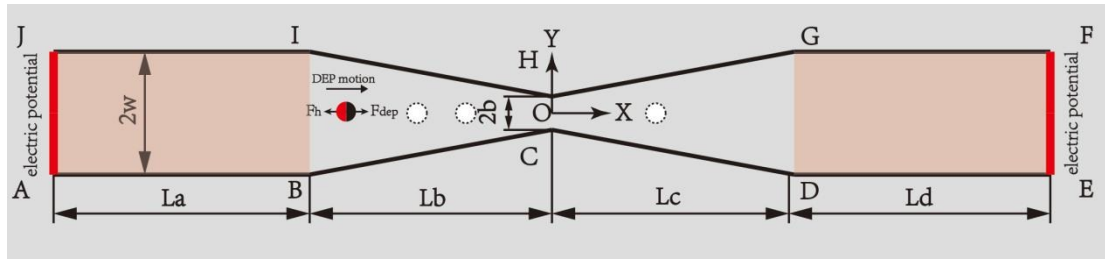


Fig. 1. A Janus particle suspended in a fluid domain under an externally applied electric field  $E^*$ . The origin of the 2D Cartesian coordinate system is located at the center of the throat.

A spherical Janus particle is suspended in a micro-channel with a symmetrical structure, and the origin of the 2D Cartesian coordinate system is located at the symmetric channel center. The micro-channel consists of three sections: a uniform inlet section, a uniform outlet section, and a converging-diverging constriction, as shown in Fig. 1. The constriction section is generated by two symmetric trapezoids, and the center of the whole structure is defined as the throat part. The computational domain includes  $\Omega$  the electric field and fluid field. An electric potential is applied on boundaries AJ and EF to generate the electric field, and the fluid is regarded as an incompressible Newtonian fluid. The Janus particle suspended in the fluid field consists of two hemispheres with different zeta potentials, and different colors are used to represent the different electrical properties.

The EDL near the polarized particle surface and the channel wall are very thin compared to the particle radius and the width of the channel, so the thin EDL approximation is applied. Therefore, the electric potential follows the Laplace equation:

$$\nabla^2 \phi = 0 \text{ in } \Omega. \quad (1)$$

The electric field obeys the following equation:

$$\mathbf{E} = -\nabla \phi \text{ in } \Omega, \quad (2)$$

The electric potential is applied on the boundaries AJ and EF:

$$\phi = \phi_0 \text{ on AJ}, \quad (3)$$

$$\phi = 0 \text{ on EF}. \quad (4)$$

The particle surface  $\Gamma_p$  and channel wall  $\Gamma_w$  are regarded as insulation boundaries, and the electric insulation boundaries can be described as follows:

$$\mathbf{n} \cdot \nabla \phi = 0 \text{ on } \Gamma \text{ and other boundaries,} \quad (5)$$

where  $\mathbf{n}$  is an outward unit normal vector. In this micro-scale study, the fluid is regarded as a creeping flow, and the Reynolds number is very small, so the inertia item can be neglected in the Navier-Stokes equation, and the fluid flow is governed by:

$$\nabla \cdot \mathbf{u} = 0 \text{ in } \Omega_f, \quad (6)$$

$$\rho_f \frac{\partial \mathbf{u}}{\partial t} = \nabla \cdot [-p\mathbf{I} + \mu(\nabla \mathbf{u} + \nabla \mathbf{u}^T)] \text{ in } \Omega_f, \quad (7)$$

where  $\mathbf{u}$  is fluid velocity,  $\mathbf{I}$  is the unit tensor,  $\nabla \mathbf{u}^T$  is the transpose of the velocity gradient, and  $\rho_f$ ,  $p$ , and  $\mu$  represent the fluid density, pressure, and dynamic viscosity, respectively.

The segments AJ and EF are selected as the inlet and outlet of the micro-channel, and an open boundary condition is applied at the two boundaries, which is given as:

$$\nabla \cdot [-p\mathbf{I} + \mu(\nabla \mathbf{u} + \nabla \mathbf{u}^T)] = 0 \text{ on AJ and EF.} \quad (8)$$

The electroosmotic flow (EOF) velocity of the channel wall can be described as:

$$\mathbf{u}_w = \frac{\varepsilon_f \zeta_w}{\mu} (\mathbf{I} - \mathbf{nn}) \cdot \nabla \phi \text{ on } \Gamma_w, \quad (9)$$

where  $\varepsilon_f$  and  $\zeta_w$  represent the fluid permittivity and zeta potential of the channel wall, respectively.

The velocity of the Janus particle consists of two parts: the Smoluchowski slip velocity and the velocity result from the particle DEP motion, which is given as:

$$\mathbf{u}_p = \frac{\varepsilon_f \zeta_p}{\mu} (\mathbf{I} - \mathbf{nn}) \cdot \nabla \phi + \frac{\partial \mathbf{S}}{\partial t} \text{ on } \Gamma_p, \quad (10)$$

where  $\zeta_p$  and  $\mathbf{S}$  represent the zeta potential and displacement of the Janus particle, and  $\mathbf{S}$  can be calculated by:

$$\rho_p \frac{\partial^2 \mathbf{S}}{\partial t^2} - \nabla \cdot \boldsymbol{\sigma}(\mathbf{S}) = 0 \text{ in } \Omega_p, \quad (11)$$

$\rho_p$  and  $\boldsymbol{\sigma}(\mathbf{S})$  represent the particle density and the Cauchy stress tensor, which is considered as a function of the Janus particle displacement.

The total force on the particle-fluid surface can be calculated by:

$$\boldsymbol{\sigma}_p \cdot \mathbf{n}_p = \boldsymbol{\sigma}_f \cdot \mathbf{n}_f + \boldsymbol{\sigma}_E \cdot \mathbf{n}_f, \quad (12)$$

$$\boldsymbol{\sigma}_f = -p\mathbf{I} + \mu(\nabla \mathbf{u} + \nabla \mathbf{u}^T), \quad (13)$$

$$\boldsymbol{\sigma}_E = \varepsilon_f \mathbf{E} \mathbf{E} - \frac{1}{2} \varepsilon_f (\mathbf{E} \cdot \mathbf{E}) \mathbf{I}, \quad (14)$$

Maxwell

where  $\boldsymbol{\sigma}_p$ ,  $\boldsymbol{\sigma}_f$ , and  $\boldsymbol{\sigma}_E$  represent the total stress tensor, hydrodynamic stress tensor, and stress tensor, respectively.

The half-width of the throat part  $b$ , zeta potential of the channel wall  $\zeta_w$ , and the electrophoretic velocity  $U_\infty = (\varepsilon_f \zeta_w / \mu)(\zeta_w / b)$  are selected as the characteristic length, characteristic electric potential, and characteristic velocity to normalize the corresponding quantities in the governing equations. The time  $t$  and electric field  $\mathbf{E}$  can be scaled by the dimensionless parameters  $\zeta_w / b$  and  $b / ((\varepsilon_f \zeta_w / \eta)(\zeta_w / b))$ . For precise calculation, the ALE method is used to solve the electric field, fluid field, and solid Janus particle simultaneously. Based on the ALE method, the finite-element mesh deforms while the Janus particle undergo the DEP motion. The computational method is identical to that used in previous studies for plain particles, where rigorous code validations are presented [13, 19, 24].

### 3. Results and discussion

This section discusses the motion and variation of a Janus particle through the converging-diverging section. The discussion can be divided into three parts: the variation of velocity and DEP force, the self-rotation phenomenon of the Janus particle, and the impact factors of the Janus particle DEP motion. To neglect the particle's gravity, the density of particles is set to be the same as the fluid,  $\rho_p = \rho_f = 1.0 \times 10^3 \text{ kg/m}^3$ , and the fluid dynamic viscosity to be  $\eta = 1.0 \times 10^{-3} \text{ kg/(m}\cdot\text{s)}$ . The permittivity and conductivity are set as  $\epsilon_f = 80\epsilon_0$  and  $\sigma_f = 2.0 \times 10^{-2} \text{ S/m}$ , respectively. Considering the effects of the channel wall, the length of the inlet and outlet sections are set to be sufficiently long to be  $L_a = L_d = 1000 \text{ }\mu\text{m}$ , the contraction part is  $L_b = L_c = 400 \text{ }\mu\text{m}$ , and the half-width of the throat is  $b = 27.5 \text{ }\mu\text{m}$ . The zeta potential  $\zeta_w = -80 \text{ mV}$  of the channel is selected for straightforward comparison with other reports for plain particles and experimental values.

### 3.1 Variation of velocity and DEP force

The Janus particle is initially located at  $(x, y) = (-0.2 \cdot L_b, 0)$  with an external electric field  $E^* = 18$ . The particle radius is  $a^* = 0.4$ , and the half-width of the uniform channel is  $w = w^* \cdot b$ , where  $w^* = 5.9$ , which is the critical dimensionless width. In order to investigate the DEP motion of the Janus particle with different zeta potential ratios (the left hemisphere zeta potential versus the right), the gamma value of the left particle hemisphere is set as a constant quantity  $\gamma_1 = 0.3$  (the corresponding zeta potential is  $\zeta_{p1} = \gamma_1 \zeta_w = -0.024 \text{ V}$ ,  $\zeta_w = -80 \text{ mV}$ ). This section discusses the variation of the velocity and DEP force with different zeta potential ratios (the ratio of the gamma values instead in this paper),  $r = -1, 0$ , and  $1$ , as shown in Fig. 2.

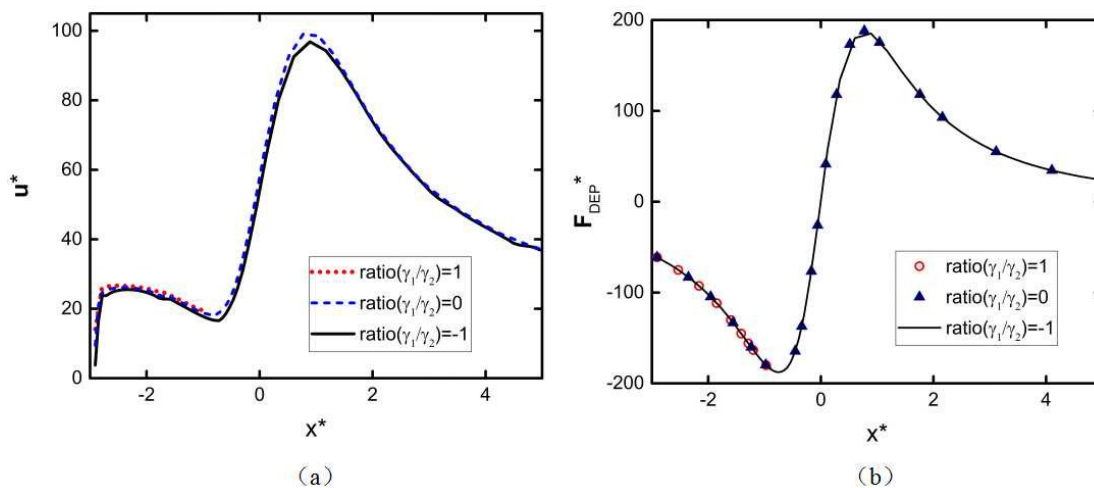


Fig. 2. The x-component velocity (a) and DEP force (b) of the Janus particle, where  $E^*=18$ ,  $w^*=5.9$ ,  $a^*=0.4$ , and  $\gamma_1=0.3$ . The solid line, dashed line, and dotted line represent the ratios  $r=\gamma_1/\gamma_2=-1, 0$ , and  $1$ , respectively.

As shown in Fig. 2a, the velocity profiles indicate whether or not the Janus particles pass through the throat part. The particles with ratios of  $r=-1$  or  $0$  can successfully pass the throat, but when the ratio gradually becomes  $r=1$ , the particles is blocked at the converging section. Before the particles pass the throat, the x-component velocity continually decreases, and once the particles successfully pass the throat, the velocity increases rapidly. When the particles move a certain distance in the diverging section, the velocity decreases again. The particle velocity consists of two parts—the Smoluchowski slip velocity and the DEP velocity—but the change of the zeta potential  $\zeta_p$  only has an effect on the former. Therefore, the gap between the solid line and dashed line represents the difference result from changing  $\zeta_p$ .

The variation of velocity can be explained by the force graph, as shown in Fig. 2b. The change of the zeta potential does not affect the DEP force, so in an identical electric field, the graphs of the DEP force coincide with each other as long as a particle with on identical radius can pass the throat. An identical DEP velocity is produced accordingly. With the change of the electric field and channel geometry, Janus particles with different sizes and electric properties are blocked at the converging section, which is called the choking phenomenon. Based on this principle, different Janus particles can be separated.

Considering actual situations, particles suspended off the channel center line are considered (e.g.,  $y^*=1.2b$ ), as shown in Fig. 3. While the particles can initially be located off the center line of the channel, the y-component of the DEP force comes into play, and the x-component of the DEP force is also different from that for the particle in the center ( $y^*=0$ ). Regardless of the initial position, however, the variation of the DEP force follows a similar scenario. The x-component of the DEP force decreases when the particle moves in the converging section. As the particle approaches the throat, the DEP force increases until the particle successfully passes through the throat. The y-component of the DEP force keeps decreasing during the entire DEP motion. When the particle moves a certain distance before the throat, the y-component of the DEP force decreases to zero, and the particle moves along the center line of the channel.



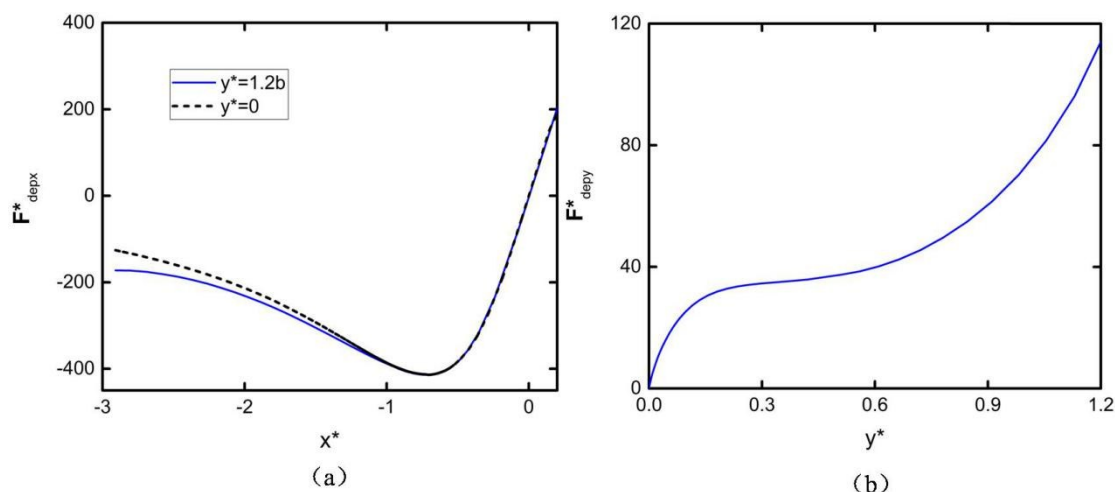


Fig. 3. The x-component (a) and y-component (b) of the DEP force of the Janus particle, where  $E^*=16$ ,  $w^*=5.9$ ,  $a^*=0.5$ ,  $\gamma_1=0.3$ , and  $\gamma_2=-0.3$ . The solid line and dashed line represent the initial y-component positions  $y^*=0$  and  $1.2b$ , respectively.

### 3.2 The self-rotation phenomenon

Compared to general particles, Janus particles have a rotation velocity that results from the different surface electrical properties. This section investigates the self-rotation phenomenon of Janus particles suspended in the fluid field with an external non-uniform electric field. The numerical simulation results show that the particles with different suspended directions keep rotating until they reach steady state, as shown in Fig. 4.

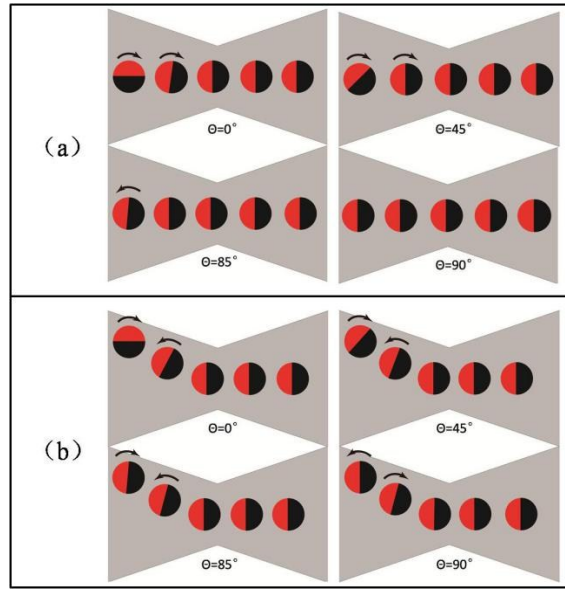


Fig. 4. The DEP motion trajectories of the Janus particle, where  $E^*=16$ ,  $w^*=5.9$ ,  $a^*=0.5$ ,  $\gamma_1=0.3$ , and  $\gamma_2=-0.3$ . The red hemisphere and black hemisphere represent  $\gamma=\gamma_1$  and  $\gamma_2$ , respectively. Initial y-component positions (a)  $y^*=0$  and (b)  $y^*=1.2b$ .

Fig. 4a and Fig. 4b show the particles with initial y-axis values of 0 and 1.2b, respectively. The angles  $\theta$  between the boundary lines inside the Janus particles and the electric field direction are set as  $0^\circ$ ,  $45^\circ$ ,  $85^\circ$ , and  $268^\circ$ . As shown, whatever the initial angles are, the Janus particles eventually rotate to  $\theta=90^\circ$  and go through the throat with this angle.

Next, the variations of rotation velocity are examined, as shown Fig. 5. Particles that are located at the center line of the channel have a regular rotation velocity. When the particles are at angles of  $\theta=0^\circ$  and  $\theta=45^\circ$ , they rotate clockwise (negative velocity value), and a particle at  $\theta=0^\circ$  has a faster rotation velocity. But when the particles are at an angle close to  $90^\circ$ , such as  $85^\circ$ , they rotate anti-clockwise and reach steady state in a short period. Furthermore, the particles at  $\theta=90^\circ$  have no rotation velocity.

Particles that are initially located above the center line have a similar tendency, as shown in Fig. 5b. The particles at  $\theta=0^\circ$ ,  $45^\circ$ ,  $85^\circ$ , and  $90^\circ$  have similar motion processes in that they rotate clockwise first and then anti-clockwise or undergo an opposite process and finally reach steady state. But at  $\theta=268^\circ$ , the particles present a larger rotation velocity and a longer distance before approaching steady state, although finally they also move along the center line. A

conclusion can be deduced that whatever the initial suspended angles are, the particles will finally rotate to the stationary direction of  $\theta=90^\circ$ , which is defined as the steady state of the Janus particle in this micro-channel. based on this principle, manipulation of the Janus particle is achieved.

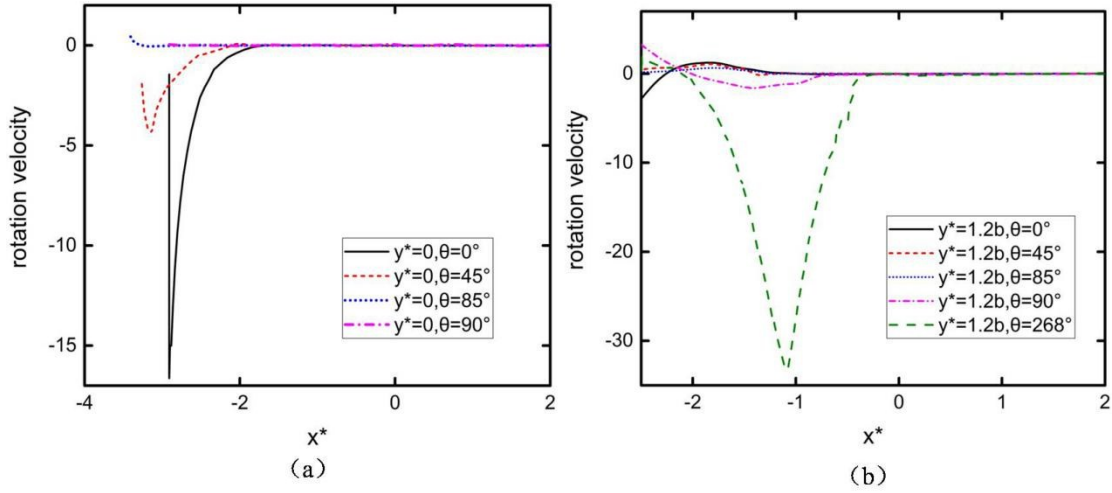


Fig. 5. The rotation velocity of the Janus particle, where  $E^*=16$ ,  $w^*=5.9$ ,  $a^*=0.5$ ,  $\gamma_1=0.3$ , and  $\gamma_2=-0.3$ . The solid line, dashed line, dotted line, and dash-dotted line represent the angle  $\theta=0^\circ$ ,  $45^\circ$ ,  $85^\circ$ , and  $90^\circ$  respectively. Initial y-component positions: (a)  $y^*=0$ , (b)  $y^*=1.2b$ .

### 3.3 Impact factors analysis

#### 3.3.1 Particle radius

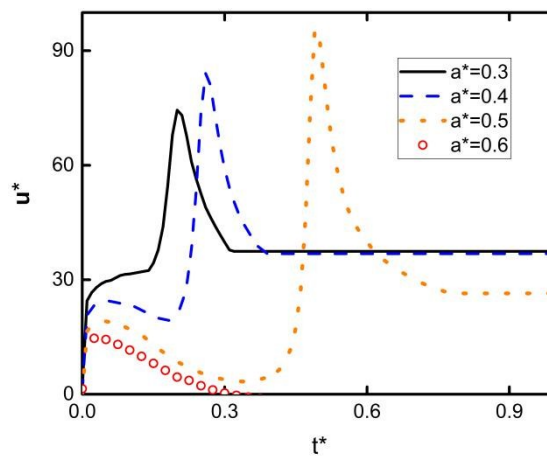


Fig. 6. The x-component velocity as a function of  $t^*$ , where  $E^*=16$ ,  $w^*=5.9$ ,  $\gamma_1=0.3$ , and  $\gamma_2=-0.3$ . The solid line, dashed line, dotted line, and circles represent particle radius  $a^*=0.3$ , 0.4, 0.5, and 0.6, respectively.

Particle size can affect the distortion of the electric field and cause different trajectories of DEP motion, as shown in Fig. 6. The Janus particles with smaller radius go through the throat in a shorter time, and as the particle radius increases, the DEP motion takes a longer period of time, and the particle is even blocked in the converging section. Smaller particles have little electric field distortion around the particle surface, resulting in a lower degree of charge polarization and thus lower DEP force. Before the particles pass the throat, the DEP force is a repelling force, but once the particles pass the throat successfully, the DEP force promotes the particle motion.

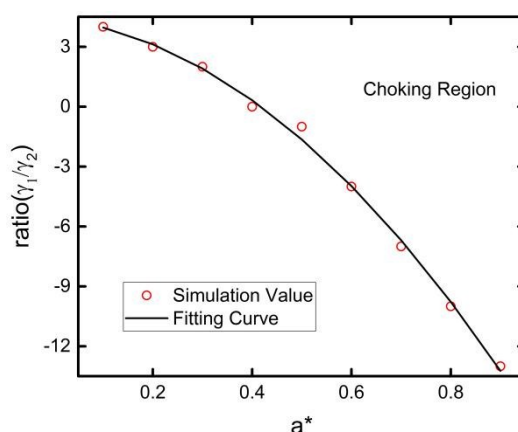


Fig. 7. DEP choking region at ratio  $r=\gamma_1/\gamma_2$  vs. particle radius  $a^*$ , where  $E^*=17.19$ ,  $w^*=5.9$ , and  $\gamma_1=0.3$ . The line and symbols represent the fitting curve and simulation values, respectively. The choking region is noted.

The choking region of Janus particles with different radii was examined, as shown in Fig. 7. In order to match previous reports [13, 19, 24],  $\gamma_1=0.3$  was used to mimic common biological cells, while the zeta potential for the other hemisphere was varied until no further significant changes were observed. For the Janus particles with  $\gamma_1=0.3$ , larger particles need a smaller zeta potential ratio to through the choking part. In a certain electric field, larger particles with an identical zeta potential require an expanded choking region. For Janus

particles with identical size and constant left gamma value, when the gamma value of another hemisphere changes, the particles are gradually blocked in the converging section. Based on this phenomenon, Janus particles with different sizes or electric properties can be separated.

### 3.3.2 Electric field

Fig. 8 shows the choking regions with different electric field strengths. For the particles with  $a^*=0.82$  and  $\gamma_1=0.3$ , a lower ratio  $\gamma_1/\gamma_2$  and higher electric potential strength result in an expanded choking region. Whatever the particle size and electric properties are, the electric field for the choking region increases nearly linearly with the decrease of the zeta potential ratio. When the surface electric properties of the particles are the same and the electric field strength is increasing, the particles are gradually blocked at the converging section. At a certain electric field strength, the Janus particles with low zeta potential ratio pass the throat part easily, so the electric field strength can be adjusted to separate different Janus particles.

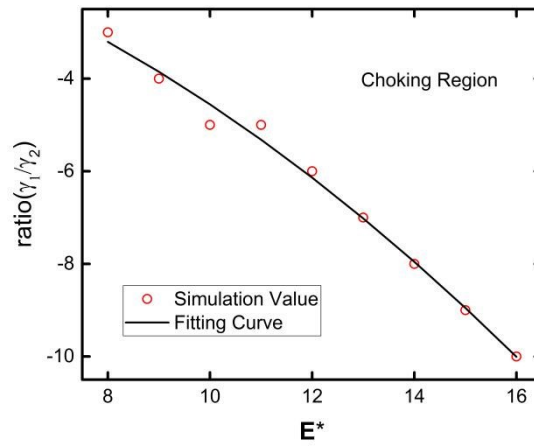


Fig. 8. DEP choking region at a ratio of  $r=\gamma_1/\gamma_2$  vs. electric field strength  $E^*$ , where  $w^*=5.9$ ,  $a^*=0.82$ , and  $\gamma_1=0.3$ . The line and symbols represent the fitting curve and simulation values, respectively.

### 3.3.3 Particle radius versus electric field

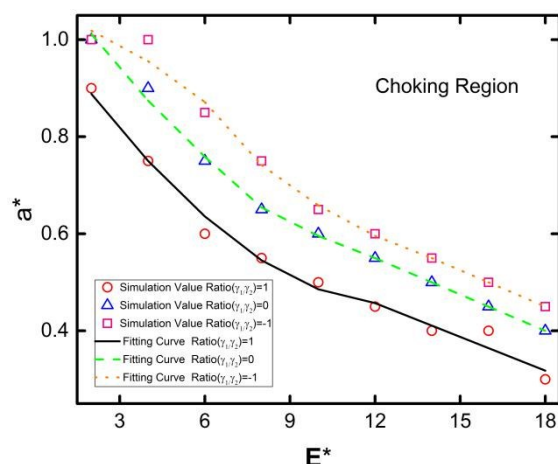


Fig. 9. DEP choking regions with particle radius  $a^*$  vs. electric field strength  $E^*$ , where  $w^*=5.9$  and  $\gamma_1=0.3$ . The lines and symbols represent the fitting curves and simulation values, respectively. The solid lines, dashed lines, and dotted lines represent  $r=\gamma_1/\gamma_2=-1, 0$ , and  $1$ , respectively.

In common experiments, the Janus particles usually have various sizes and surface electric properties, so the choking phenomenon of Janus particles with different radiuses and electric potential ratios is studied simultaneously, as shown in Fig. 9. For particles with any zeta potential ratio  $r=\gamma_1/\gamma_2=-1, 0$ , or  $1$ , a smaller particle needs a higher electric strength for the converging section to block it. When the gamma value of one hemisphere is constant at  $\gamma_1=0.3$  and the zeta potential ratio is increasing, the choking region is expanded. But when the particle radius increases to a certain value of  $a^*=1.0$ , the choking region does not change as the electric field strength decreases, so the boundaries of the choking region have an intersection, as shown in Fig. 9. The results coincide with the discussions thus far, and the Janus particles with different sizes and electric properties can be separated by adjusting the applied electric field.

#### 4. Concluding remarks

Numerical simulation studies of Janus particles that are being transported electrokinetically provide guidance for non-uniform particle manipulation. A converging-diverging structure can be used more efficiently for non-uniform particles for separation and concentration based on the presented results. An ALE method was used to

determine the motion of Janus particles suspended in a coupled electric field and flow field, and the MST method was employed to calculate the DEP force accurately.

The simulation results show that a constriction structure can indeed block Janus particles in the converging section, but with different criteria from those for uniform particles. Regardless of the initial orientation of the Janus particles, they rotate themselves to achieve the most favorable angle of  $\theta=90^\circ$  with respect to the applied electric field. The parametric studies showed that particle size and electric properties affect the Janus particles' DEP motion, and when the particle radius or applied electric field strength increases, the choking region gradually expands. Thus, the applied electric field strength can be adjusted to block or promote the Janus particle DEP motion.

Based on the choking and self-rotation phenomenon, the separation and manipulation of Janus particles may be achieved. For much smaller nano-scale Janus particles, more detailed studies are required to resolve the effect of the EDL surrounding the particle surface. This study presented a theoretical prediction that a Janus particle can circumvent the choking phenomenon to an extent by rotating itself for the first time, but the results should be verified experimentally.

## ACKNOWLEDGMENT

This work was funded by the central government guiding special funds for the development of local science and technology (ZY2018HN09-6), the National Natural Science Foundation of China (Grant No. 51605124 and 51875545), the Scientific Research Foundation of Hainan University (Grant No. Kyqd1569, hdkyxj201721 and hdkyxj201722), and the National Research Foundation of Korea (Grant NRF-2018R1A2B3001246).

*The authors have declared no conflict of interest.*

## 5 References

- [1] Kang, Y., Li, D., Kalams, S. A., Eid, J. E., *Biomed. Microdevices* 2008, 10, 243-249.
- [2] Hyoung Kang, K., Xuan, X., Kang, Y., Li, D., *J. Appl. Phys.* 2006, 99, 810.
- [3] Barbulovicnad, I., Xuan, X., Lee, J. S., Li, D., *Lab Chip* 2006, 6, 274-279.
- [4] Xuan, X., Zhu, J., Church, C., *Microfluid. Nanofluid.* 2010, 9, 1-16.
- [5] Zhou, T., Shi, L., Fan, C., Liang, D., Weng, S., Joo, S. W., *Microfluid. Nanofluid.* 2017, 21, 59.
- [6] Zhou, T., Xu, Y., Liu, Z., Joo, S. W., *J. Fluids Eng.* 2015, 137, 091102.
- [7] Ai, Y., Park, S., Zhu, J., Xuan, X., Beskok, A., Qian, S., *Langmuir* 2010, 26, 2937-2944.
- [8] Zhou, T., Liu, T., Deng, Y., Chen, L., Qian, S., Liu, Z., *Microfluid. Nanofluid.* 2017, 21, 11.
- [9] DuBose, J., Lu, X., Patel, S., Qian, S., Joo, S. W., Xuan, X., *Biomicrofluidics* 2014, 8, 014101.
- [10] Ai, Y., Joo, S. W., Jiang, Y., Xuan, X., Qian, S., *Electrophoresis* 2009, 30, 2499-2506.
- [11] Ai, Y., Mauroy, B., Sharma, A., Qian, S., *Electrophoresis* 2011, 32, 2282-2291.
- [12] Xuan, X., Xu, B., Li, D., *Anal. Chem.* 2005, 77, 4323-4328.
- [13] Zhou, T., Ge, J., Shi, L., Fan, J., Liu, Z., Woo Joo, S., *Electrophoresis* 2018, 39, 590-596.
- [14] Ai, Y., Qian, S., Liu, S., Joo, S. W., *Biomicrofluidics* 2010, 4, 13201.
- [15] Zhu, J., Xuan, X., *Electrophoresis* 2009, 30, 2668-2675.
- [16] Walther, A., Mä%Ller, A. H., *Chem. Rev.* 2013, 113, 5194-5261.
- [17] Boymelgreen, A., Yossifon, G., *Langmuir* 2015, 31, 8243-8250.
- [18] Zhao, K., Li, D., *J. Micromech. Microeng.* 2017, 27, 095007.
- [19] Zhou, T., Liu, Z., Wu, Y., Deng, Y., Liu, Y., Liu, G., *Biomicrofluidics* 2013, 7, 054104.
- [20] Ai, Y., Qian, S., *J. Colloid Interface Sci.* 2010, 346, 448-454.
- [21] Ai, Y., Qian, S., *Phys. Chem. Chem. Phys.* 2011, 13, 4060-4071.



---

[22] Ai, Y., Zeng, Z., Qian, S., *J. Colloid Interface Sci.* 2014, 417, 72-79.

[23] Hirt, C. W., Amsden, A. A., Cook, J. L., *J. Comput. Phys.* 1974, 14, 227-253.

[24] Zhou, T., Deng, Y., Zhao, H., Zhang, X., Shi, L., Woo Joo, S., *J. Fluids Eng.* 2018, 140, 091302-091302-091306.